J. Astron. Space Sci., Vol. 6, No. 1, 1−15(1989)

THREE DIMENSIONAL COMPUTER MODELING OF MAGNETOSPHERIC SUBSTORM

Kyoung W. Min
Korea Institute of Technology, Taejon 302-338, Korea
(Received March 1, 1989 ; Accepted May 31, 1989)

Abstract

Magnetospheric substorm in the magnetotail region is studied numerically by means of a three dimensional MHD code. The analytic solution for the quiet magnetotail is employed as an initial configuration. The localized solar wind is modeled to enter the simulation domain through the boundaries located in the magnetotail lobe region. As a result of the interaction between the solar wind and the magnetosphere, the magnetic field lines are stretched, and the plasma sheet becomes thinner and thinner. When the current driven resistivity is generated, magnetic reconnection is triggered by this resistivity. The resulting plasma jetting is found to be super-magnetosonic. Although the plasmoid formation and its tailward motion is not quite clear as in the two dimensional simulation, which is mainly because of the numerical model chosen for the present simulation, the rarification of the plasmas near the x-point is observed. Field aligned currents are observed in the late expansive stage of the magnetospheric substorm. These field aligned currents flow from the tail toward the ionosphere on the dawn side and from the ionosphere toward the tail on the dusk side, namely in the same sense of the region 1 current. As the field aligned currents develop, it is found that the cross tail current in the earth side midnight section of the magnetic x-point is reduced.

1. Introduction

Magnetic reconnection in the tail is widely believed to be the direct cause of magnetospheric substorms. Based on observational evidence, a phenomenological model of substorms in the tail has been developed(Hones, 1977). In this near-earth neutral line model, reconnection on the dayside magnetopause is followed by the formation of a new neutral line in a localized region in the near-earth plasma sheet(McPherron *et al.*, 1973). On the

earthside of the neutral line, the plasma sheet thickens and the magnetic field becomes more dipolar. The earthward plasma sheet is characterized by earthward flow and a northward magnetic field. On the tailward side of the neutral line, the plasma sheet thins as a magnetic bubble flows tailward away from the earth.

Several observational studies have inferred a localized transient field aligned current system near midnight during substorms(Akasofu and Meng, 1969; McPherron *et al.*, 1973). This current flows into the ionosphere on the morning side and away on the evening side and is believed to be connected to the westward electrojet in the ionosphere. Atkinson (1966) suggested that such a current system would result from localized reconnection in the magnetotail and Sato(1982) has developed a model for the resulting field aligned currents based on his simulation.

Several numerical magnetohydrodynamic(MHD) models of reconnection in the tail have been developed. These include studies of tearing mode reconnection(Birn and Hones, 1981 ; Sato and Walker, 1982 ; Forbes and Priest, 1983) and studies of driven magnetic reconnection(Sato, 1979; Min *et al.*, 1985). Birn and Hones(1981) presented a three dimensional simulation of tail dynamics. Starting with self-consistent tail models(Birn, 1979), they solved the MHD equations throughout the tail. In this calculation, the tearing mode instability was driven by a sudden increase in resistivity. The calculation reproduced many of the features of the near-earth neutral line model. After the resistivity was turned on, the plasma sheet began thinning and an x-type neutral line formed. A bubble formed tailward of the neutral line and began moving down the tail. The field aligned currents were observed to be directed tailwards on the dawnside and toward the earth on the duskside. They suggested that their current system was responsible for the substorm associated changes in the region 2 currents of Iijima and Potemra(1978).

In the present paper, the results of the driven reconnection calculations in the three dimensional model of magnetospheric substorm are reported. In particular, I will discuss the changes in the magnetospheric currents which result from driven reconnection with emphasis on the generation of field aligned currents. I will also discuss the plasma flows which result from driven reconnection. These results will be compared with the results of the observation.

2. Numerical Model

In the two dimensional study(Min *et al.*, 1985), the dipole magnetic field was used as an initial configuration along with the constant pressure everywhere. This dipole field was developed into a tail-like configuration as a result of interaction with the solar wind. Subsequent evolution of the magnetotail including magnetic reconnection can be modeled self-consistently.

Limitations of computer time and memory put even more severe restrictions on the three dimensional study than the two dimensional one. Thus, instead of starting with a three dimensional dipole field, a three dimensional analytic solution for tail-like configuration is used as an initial condition. At present time there is no exact solution available for the magnetophere in static equilibrium. However, Birn and his colleagues(1977a, 1977b, 1979) developed an asymptotic solution for the magnetotail region assuming the smallness of the north-south component of the magnetic field and the variations in the sun-earth direction as well as in the dawn-dusk direction. The result is

$$P = q\frac{1}{\cosh^2\left(\frac{\sqrt{2q\lambda}}{|\nabla\beta|}z\right)} \quad \cdots\cdots (1)$$

$$B_x = \frac{-160}{x+140}\left(\tanh\left(\frac{\sqrt{2q\lambda}}{|\nabla\beta|}z\right)\right)\frac{\sqrt{2q}}{|\nabla\beta|} \quad \cdots\cdots (2)$$

$$B_y = \frac{-160y}{(x+140)^2}\left(\tanh\left(\frac{\sqrt{2q\lambda}}{|\nabla\beta|}z\right)\right)\frac{\sqrt{2q}}{|\nabla\beta|}, \quad \cdots\cdots (3)$$

where $\beta = \frac{160y}{(x+140)}$, $q = q_0 \cdot |x|^{-12}$, and B_z is calculated numerically.

For the present study $\lambda = 0.4$ is taken. $q_0 = 0.1 \times 160^{12}$ is a nomalization constant. Here, x, y, and z are normalized by $1R_E(=6{,}400km)$. Figure 1 shows the configuration of the equilibrium calculated in this way: (a) the magnetic field configuration, and (b) the pressure distribution. In the present study the simulation domain is located deep inside the magnetosphere, i.e., $20 \leq x \leq 80$, $-10 \leq y \leq 10$, and $-12 \leq z \leq 12$. Although there is a finite B_y

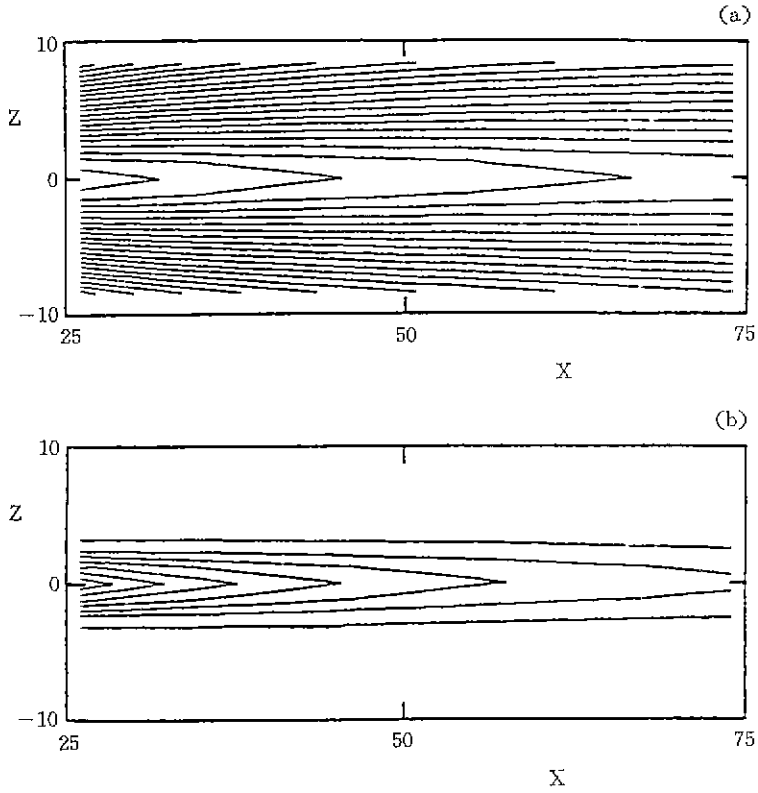

Fig. 1. Noon-midnight meridian cross section of the three dimensional analytic solution for the quiet magnetosphere : (a) magnetic field lines. and (b) pressure distribution.

component which varies in the dawn-dusk direction, other quantities such as B_x , B_z, and P do not vary much in the y-direction, in contrast to the initial configuration for the simulation study by Birn and Hones(1981) where the pressure increases toward the flank of the tail. This is due to our choice of free parameters. However, since we are concerned about the central regin of the tail, and the model involves plasma entry from the external source(solar wind), the initial variation in the dawn-dusk direction may not be so relevant to the substorm expansive stage as far as the present model is concerned.

To fit our choice of parameters quantitatively to the observed values(Fairfield, 1979) the normalized magnetic field intensity B_0 is taken to be 2.5×10^{-4} Gauss. Then, the nor-

malized pressure, $P_0 = \frac{B_0^2}{2\mu_0}$, is determined to be 2.4×10^{-9} dynes/cm^2. At this point we have freedom to choose the density and the temperature distribution as long as they give the same pressure values determined by the equation (1). In this simulation the density is given uniformly at the value n(number density) = 0.5/cm^3, or the mass density $\rho = 8.35 \times 10^{-25}$g/cm^3, and the temperature is determined accordingly. With this choice the temperature at x = 50, z = 0 is about 500eV, which is not unrealistic. Since our solution is for the static equilibrium, the plasma is initially assumed to be at rest without any macroscopic flow velocity. The normalized Alfven velocity V_{A0}=800km/sec, and the Alfven transit time $\tau_A = L/V_{A0} = 8$ sec, where L = 6,400km. In the actual calculations all variables are normalized according to the above characteristic quantities, and the discussions hereafter will be made in terms of the normalized quantities.

The usual resistive MHD equations, with the ratio of the specific heats taken to be $\frac{5}{3}$, are normalized and transformed into the two-step Lax-Wendroff scheme. Since the system is assumed symmetric about the equatorial plane and the meridian plane, the calculations are performed only for the dawn side northern hemisphere, and the mirror boundary conditions are imposed on the symmetric planes, i.e., the equatorial plane(z = 0) and the meridian plane (y = 0). Free boundary conditions are imposed on the earth side boundary(x = 20), tail side boundary(x = 80), and the dawn side boundary(y = 10). The solar wind plasma, which intrudes into the magnetosphere, presumably as a result of dayside reconnection, is modeled to enter the simulation box through the tail lobe boundaries(z = $\pm$ 12). The solar wind considered here is the plasma flow after its passage through the bow shock and the magnetopause, since the simulation region is located deep inside the magnetosphere. Thus, the solar wind in this model is not super-Alfvenic. More on the solar wind entry model will be discussed in section 3. The simulation box of the dawn side northern hemisphere is divided into $41 \times 22 \times 41$ grids so that the mesh size is $1.5R_E$ in the x-direction, $0.5R_E$ in the y-direction, and $0.3R_E$ in the z-direction.

3. Results

Before studying the interaction between the solar wind and the quiet magnetosphere, the asymptotic solution for the equilibrium is tested by means of the numerical simulation with the ideal MHD equations, while the variables at the boundaries are fixed at

the initial values, and it is found that the equilibrium solution is good enough to be used as an initial configuration for the present study. Until $T = 50$ there is no significant change in the configuration of the magnetic field and in the plasma sheet structure. This test run also proves that our numerical diffusion is unimportant, and we can safely separate the physical result from the numerical one.

The solar wind entry is modeled by the boundary conditions on the tail lobe boundary. Namely, for the magnetic field, $\nabla_{\perp} B_{\parallel} = 0$, and $B_{\perp}$ is determined from the solenoid condition, $\nabla \cdot B = 0$, Also,

$$\rho_1 = \rho_{initial} \frac{B_2}{B^2_{initial}} ,$$

$$P = P_{initial} \frac{B^2}{B^2_{initial}} ,$$

$$\rho V_Z = -\frac{A_0}{4} \left(1 + \cos \frac{2\pi(x - 50)}{L_X} \right) \left(1 + \cos \frac{\pi y}{L_Y}\right) ,$$

and ρV_X and ρV_y are adjusted so that the mass flow vector is always perpendicular to B at the boundary. Here, $L_X = 60$ and $L_y = 10$. A_0 is increased monotonically from 0 to 0.2 in $10\tau_A$ and maintained at the same value thereafter. The resulting plasma flow velocity is sub-Alfvenic everywhere on the tail lobe boundary.

When the interplanetary magnetic field is oriented southward, dayside reconnection is enhanced and the entry of the solar wind plasma can be thought to be localized in the meridian plane, rather than being thought to be broad over the entire dawn-dusk direction. Also, the observational fact that the plasma sheet thinning before the onset of the substorm expansive phase is frequently detected at the distance less than $15R_E$, while the Vela satellites at $x \sim 18R_E$ do not usually observe the thinning implies that the spatial extent of the thinning region is rather limited. In the discussion of the previous two dimensional simulation result(Min *et al.*, 1985) it was argued that the plasma sheet thinning is due to the solar wind stresses. Thus, the limited spatial extent of the plasma sheet thinning in the x-direction may come from the spatially localized solar wind stresses in the x-direction. The present particular plasma entry model is chosen in view of such localization of the solar wind flux in both the x- and y-direction.

Since we assume magnetic reconnection as a mechanism for the magnetospheric substorm, we need plasma resistivity which will trigger magnetic reconnection, with the assumption of the resistive Ohm's law. The resistivity in this study is assumed to have the following form, as in the two dimensional study,

$$\eta = \begin{cases} \alpha(J - J_C)^2 \text{ if } J > J_C \ ; \\ 0 \qquad\qquad \text{otherwise} \end{cases}$$

where α is a numerical parameter characterizing the current driven microscopic instability, J is the y-component of the current density, and J_C is the threshold value. Particularly, $\alpha = 0.05$, $J_C = -1.0$, and the resultant maximum value of resistivity is about 0.015 at T = 140. The dependence of the resistivity on the current density implies that our anomalous resistivity is assumed to be generated by the current driven instability(Huba *et al.*, 1977; Sato 1979; Tanaka and Sato 1981a, 1981b).

As the solar wind plasmas entering from the tail lobe boundaries move into the plasma sheet region, magnetic field lines are compressed and the plasma sheet becomes thinner. Figure 2 shows the results at T = 40: (a) the magnetic field lines on the meridian plane,

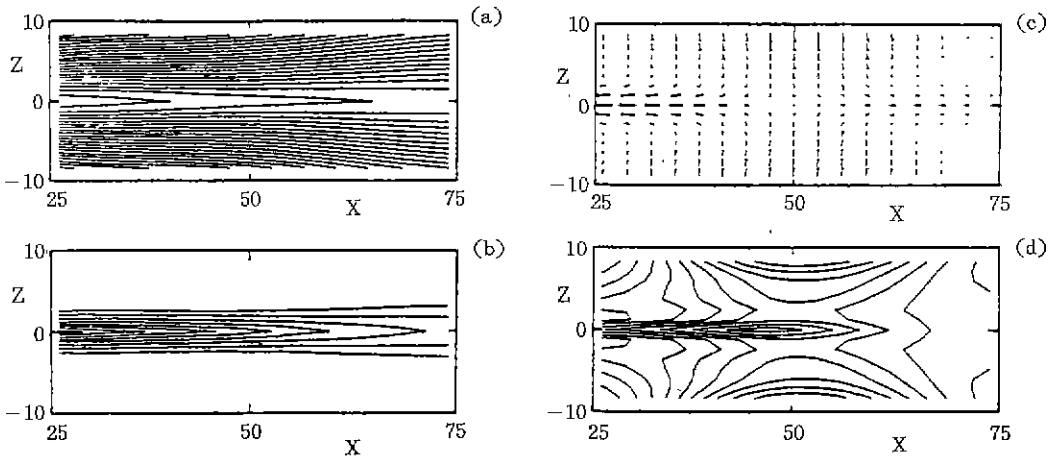

Fig. 2. Noon-midnight meridian cross section of the result at T = 40 : (a) magnetic field lines, (b) pressure distribution, (c) plasma flow velocity, and (d) density distribution.

(b) the pressure distribution on the meridian plane, (c) the plasma flow velocity on the meridian plane, (d) the density distribution on the meridian plane. The magnetic field line configuration does not change much at this time, although one can see the compression of the magnetic field lines, if one looks at the figure closely. The plasma sheet in Figure 2 (b) shows the indication of our solar wind plasma entry pattern, namely a peaked solar wind influx in the central region with the decreasing function toward the boundaries. However, it is interesting to note that the plasma sheet in the near earth region also becomes thinner, while that near the tail side boundary does not. Plasma flow velocity plotted in Figure 2 (c) shows that the plasmas entering through the tail lobe boundaries move out through the earth side boundary and the tail side boundary, as well as through the dawn and dusk boundaries(Figure 3). One interesting feature is that the plasma flow toward the earth is larger than the flow toward the tail side boundary. The reason is that the E × B dirft is in the earthward direction, with the dawn to dusk electric field penetrating from the boundaries and the northward magnetic field in the plasma sheet region. In the plot of the plasma density distribution it is seen that plasmas are piling

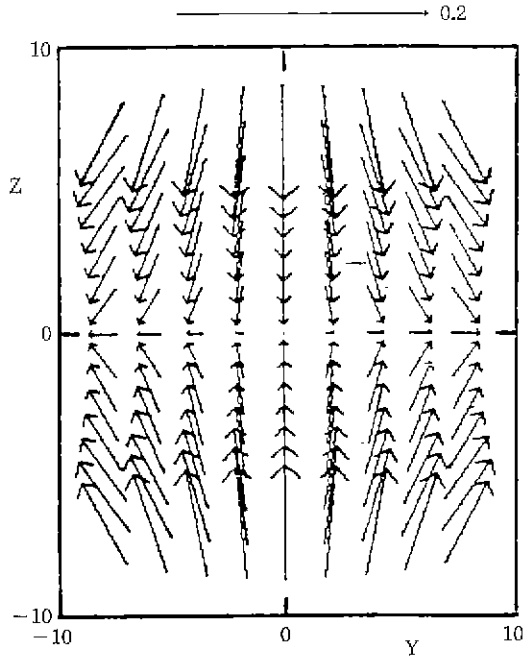

Fig. 3. Plasma flow velocity at T = 40 on the y-z plane located at $44R_E$ from the earth.

up in the central region. However, its change from the initial value is found to be less than 20 percents. Also, the high density region appears near the tail lobe boundaries due to our numerical model in which the plasmas move in through these boundaries. At this time T = 40, the resistivity is still zero everywhere, since the cross tail current density has not reached the threshold value yet.

The cross tail current density is initially peaked in the near earth region. However, as the plasma sheet thinning process and the compression of the magnetic field lines keep going on, the neutral current density near the central region($x = 50$, $z = 0$) becomes larger and the current driven resistivity is generated in this region first. Magnetic reconnection starts in this central region at about T = 70 due to the excited resistivity. When the resistivity is excited, the development of the current density is suppressed by this resistivity. Thus, the current density in the central region does not grow fast, while in the off central region, where the resistivity is not generated yet, the current density increases rapidly, and then, the resistivity is excited there, too. As a result, magnetic reconnection soon occurs everywhere up to the dawn and dusk boundaries of the present model. It should be noted that the simulation domain is located deep inside the magnetotail($-10 \leq y \leq 10$). Thus, this spatial extent of the magnetic reconnection region up to the dawn and dusk boundaries may not be unrealistic.

Figure 4 shows the result of the final stage of the simulation : (a) the magnetic field line configuration on the meridian plane, (b) the magnetic field line configuration on the plane parallel to the meridian plane and located at $y = 9$, (c) the plasma flow on the meridian plane, and (d) the density distribution on the meridian plane. The plots (a) and (b) of the magnetic field lines in Figure 4 show that the magnetic island is larger in the tail region than the earth side region of the magnetic x-point. This comes from the fact that the x-component of the magnetic field is stronger in the earth side region than the tail region, which is assumed in the initial configuration. Thus, if the magnitude of B_z is the same, since the flux transferred is the same, the smaller B_x makes larger magnetic island. Comparing the two figures of the magnetic field lines, Figures 4 (a) and 4 (b), one can see magnetic reconnection is more developed in the meridian plane than the plane located at $9R_E$ on the dawn side, since magnetic reconnection has started earlier in the central region, as discussed. Also, the magnetic x-point is closer to the earth in the dawn and dusk boundary planes than the meridian plane. This behavior was also seen in the simulation study by Birn(Figure 4 in the paper by Birn, in Magnetic Reconnection in Space and Laboratory Plasmas, edited by Hones, 1984), where the simple tea-

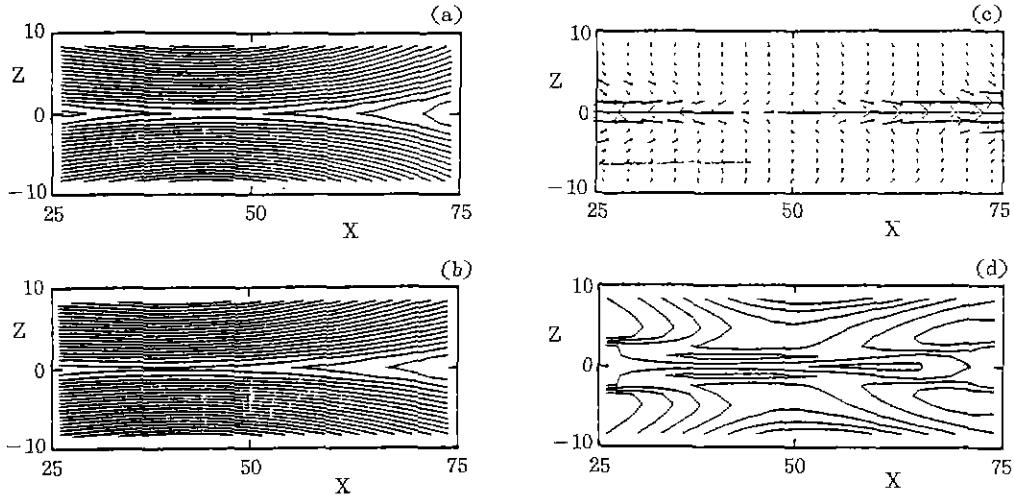

Fig. 4. Substorm expansive phase at T = 140 : (a) magnetic field lines on the noon-midnight meridian plane, (b) magnetic field lines on the plane parallel to the meridian plane and located at $9R_E$ on the dawn side, (c) plasma flow velocity on the noon-midnight merdian plane, and (d) density distribution on the noon-midnight meridian plane.

aring mode triggered magnetic reconnection.

Figure 4 (c) shows the strong plasma jetting across the x-line. In contrast to the pre-reconnection phase in which the earthward plasma flow was larger than the tailward flow, the tailward plasma jetting is now larger than the earthward plasma jetting in the reconnection phase. The tailward plasma jetting speed is as high as 1000km/sec, which is larger than the local magnetosonic speed(~ 400km/sec). Another interesting feature of the plasma flow is that the plasmas enter the simulation domain through the dawn and dusk boundaries in the reconnection phase(Figure 5), in contrast to the pre-reconnection phase in which the plasmas moved out through these boundaries. Also, the plasma velocities near the tail lobe boundaries are reduced, compared with Figure 3, although V_z is fixed at the same value on these boundaries. This effect comes from the pressure gradient toward the plasma sheet.

The plasma density at T = 140 is plotted in Figure 4 (d). The plasma density near the x-point becomes low, in contrast to the pre-reconnection phase in which the density was

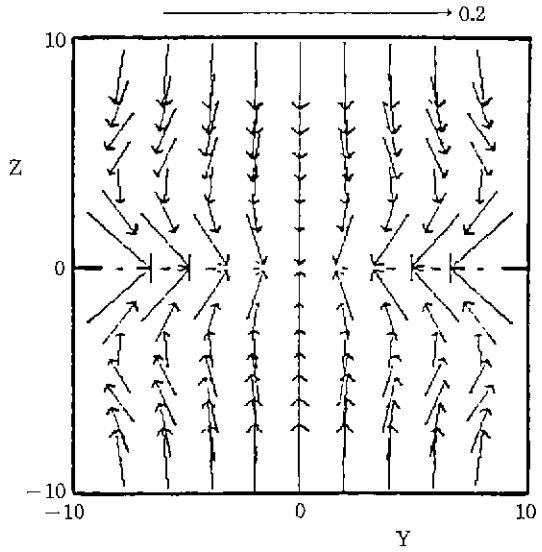

Fig. 5. Plasma flow velocity at T = 140 on the y-z plane located at $44R_E$ from the earth.

peaked near the central region(Figure 2 (d)). The peaked point of the plasma density is located at x = 63, z = 0. Plasmoid-like density distribution is shown around this peaked point. However, this bulk of plasmas is not surrounded by the closed loop of the magnetic field lines, and it should not be regarded as a plasmoid which was detected by the satellite observations and seen in the previous two dimensional simulation study. The present obscure picture of the plasmoid may be due to our numerical model in which the plasma entry boundaries(tail lobe boundaries) are too close to the plasma sheet region. However, the rarification of the plasma near the x-point indicates that the formation of the plasmoid and its motion can also arise in the three dimensional case.

The cross tail current density and the field aligned currents at T = 140 are plotted in Figure 6 : (a) the y-component of the cross tail current on the y-z plane located at x = 26, (b) the cross section of the distribution of the field at x = 26, and (c) the cross section of the distribution of the field aligned currents on the y-z plane located at x = 38. A close look at Figure 6 (a) reveals that the cross tail current is reduced in the midnight region. The field aligned currents are plotted in Figure 6 (b). Note that this plane is located in the earth side of the magnetic x-point. The magnitude of the peaked

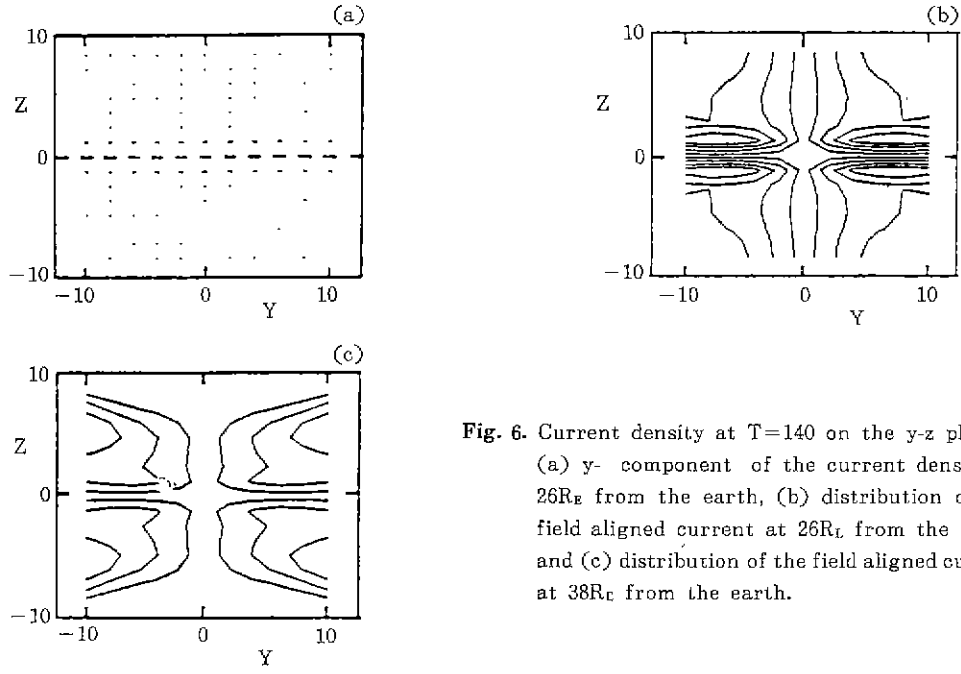

Fig. 6. Current density at T=140 on the y-z plane : (a) y- component of the current density at $26R_E$ from the earth, (b) distribution of the field aligned current at $26R_E$ from the earth, and (c) distribution of the field aligned current at $38R_E$ from the earth.

field aligned current is observed to be about 20 percent of the local value of the cross tail current. The field aligned current observed in this model has the same sense of the region 1 current, that is, it flows toward the ionosphere from the tail on the dawn side, and it flows toward the tail from the ionosphere on the dusk side. These results are opposite to those obtained in the simulation study by Birn and Hones(1981), and agree with the results studied by Sato *et al.* (1984). Also, the field aligned currents in our model are generated in the late stage of magnetic reconnection, in contrast to the case of the simple tearing mode simulation by Birn and Hones(1981) in which the field aligned currents increase rapidly until magnetic reconnection occurs and they remain more or less at the steady values afterwards.

The energy conversion due to magnetic reconnection can be studied by using Figure 7. The curve a represents the plasma acceleration and the curve b represents the Joule heating in the system. Both of the curves show sharp increases after T = 70, which implies that magnetic reconnection starts at T = 70 and it develops afterwards. In the present three dimensional study the plasma acceleration is about four times as large as the Joule heating at T = 140.

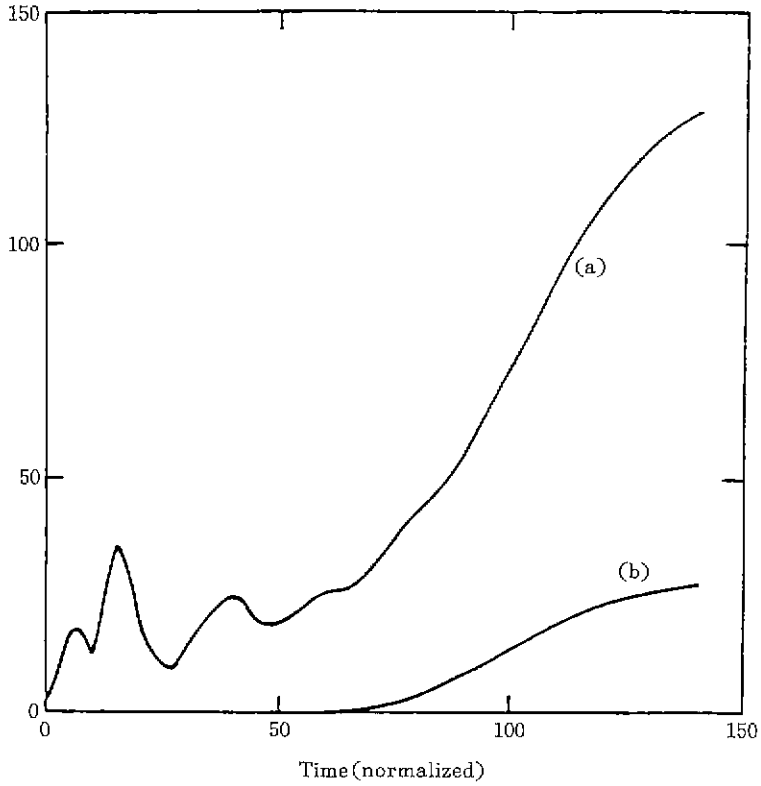

Fig. 7. Energetics of the system : (a) plasma acceleration, and (b) Joule heating.

4. Discussion

In this section the simulation results will be compared with the observations and the theoretical models. In particular, the generation of the field aligned currents and the substorm current system will be studied.

The field aligned current in the distant tail region is not well studied observationally. Frank *et al.*(1984) reported that the field aligned currents observed in the boundary layer of the plasma sheet have the region 1 current signatures. It should be noted that this observation was made during the substorm recovery phase with the ISEE-1 space-craft

located at 19.8R_E from the earth in the tail region. Thus. if magnetic reconnection should play an important role in the generation of the field aligned currents, the point of this observation can be regarded as being located in the earthward region of the x-point, since the magnetic x-point is thought to move tailward in the recovery phase.

The results of the present simulation, as discussed in section 3, show the region 1 signature of the field aligned currents : the currents flow from the tail toward the ionosphere on the dawn side and from the ionosphere toward the tail on the dusk side(Figure 6 (b)). Also, as can be seen in Figure 6 (c), there is no systematically enhanced field aligned current at x = 38. Thus, it can be argued that the field aligned currents are generated in the earthward region of the magnetic x-point, not in the region around the x-point.

These field aligned currents are diverted currents from the cross tail currents. As discussed in section 2, the cross tail current is reduced in the midnight region when magnetic reconnection is well developed. Thus, part of the current flowing into the midnight region from the dawn side is diverted and flows along the magnetic field line toward the ionosphere. This current system agrees with model made by Kamide *et al.*(1976).

The equation for the generation of the field aligned currents can the written as

$$B\frac{\partial}{\partial s}\left(\frac{J_{\parallel}}{B}\right) = \rho\frac{d}{dt}\left(\frac{\Omega}{B}\right) + \frac{2}{B}\vec{J}_{\perp}\cdot\vec{\nabla}B - \frac{1}{\rho}\vec{J}_{in}\cdot\vec{\nabla}\rho \ ,$$

where

$$\Omega = \hat{b}\cdot(\vec{\nabla}\times\vec{v}) \ ,$$
$$\vec{J}_{in} = -\frac{c\rho}{B^2}\frac{d\vec{V}}{dt}\times\vec{B} \ .$$

Applying this equation to the present study, the first term on the right hand side gives the opposite sense of the field aligned currents of the simulation results, and the last term is negligible, since $J_{in} \ll J_{\perp}$. The second term, which is positive on the dawn side and negative on the dusk side, yielding the proper sense of the field aligned currents of the simulation results, is responsible for the generation of the field aligned current in this model.

In the present model the interaction of the field aligned currents with the ionosphere is not included, since the earth side boundary is assumed as a free boundary. However,

if the magnetosphere is assumed to be the generation side of the field aligned currents and ionosphere is regarded as a dissipation side of the currents, the present simulation model is plausible and it provides at least a qualitative picture of the substorm current system.

References

Akasofu, S.-I. and Meng, C.-I. : 1969, *J. Geophys. Res.* **74**, 293.

Atkinson, G. : 1966, *J. Geophys. Res.* **71**, 5157.

Birn, J. : 1979, *J. Geophys. Res.* **84**, 5143.

Birn, J., Sommer, R. R., and Schindler, K. : 1977a, *J. Geophys. Res.* **82**, 147.

Birn, J., Sommer, R. R., and Schindler, K. : 1977b, *J. Geophys. Res.* **82**, 1964.

Birn, J. and Hones, E. W., Jr. : 1981, *J. Geophys. Res.* **86**, 6802.

Fairfield, D. H. : 1979, *J. Geophys. Res.* **84**, 1950.

Forbes, T. G. and Priest, E. R. : 1983, *J. Geophys. Res.* **88**, 863.

Frank, L. A., Huang, C. Y., and Eastman, T. E. : 1984, in *Magnetospheric Currents*, edited by T. A. Potemra, AGU, Washington D. C..

Hones, E. W., Jr. : 1977. *J. Geophys. Res.* **82**, 5633.

Huba, J. D., Gladd, N. T., and Papadopoulos, K. : 1977, *Geophys. Res. Lett.* **4**, 125.

Iijima, T. and Potemra, T. A. : 1978. *J. Geophys. Res.* **83**. 599.

Kamide, Y., Yasuhara, F., and Akasofu, S.-I. : 1976, *Planet. Space Sci.* **24**, 215.

McPherron, R. L., Russell, C. T., and Aubry, M. P. : 1973, *J. Geophys. Res.* **78**, 3131.

Min, K., Okuda, H. and Sato, T. : 1985, *J. Geophys, Res.* **90**, 1985.

Sato, T. : 1979, *J. Geophys. Res.* **84**, 7177.

Sato, T. : 1982, in *Magnetospheric Plasma Physics*, edited by A. Nishida, D. Reidel Publ. Co., Boston.

Sato, T. and Walker, R. J. : 1982, *J. Geophys. Res.* **87**, 7453.

Sato, T., Walker, R. J. and Ashour-Abdalla, M. : 1984, *J. Geophys. Res.* **89**, 9761.

Tanaka, M. and Sato, T. : 1981a, *J. Geophys. Res.* **86**, 5541.

Tanaka, M. and Sato, T. : 1981b, *Phys. Rev. Lett.* **47**, 714.